Paper
Int'l J. of Aeronautical & Space Sci. 17(1), 8–19 (2016)
DOI: http://dx.doi.org/10.5139/IJASS.2016.17.1.8

IJASS
International Journal of Aeronautical and Space Sciences

Effects of Inlet Turbulence Conditions and Near-wall Treatment Methods on Heat Transfer Prediction over Gas Turbine Vanes

Jeong-Gyu Bak* and Jinsoo Cho**

Dept. of Mechanical Engineering, Hanyang University, Seoul 04763, Republic of Korea

Seawook Lee***

Dept. of Aerospace Engineering, Ryerson University, Toronto, M5B 2K3, Canada

Young Seok Kang****

Aero Propulsion System Team, Korea Aerospace Research Institute, Daejeon 34133, Republic of Korea

Abstract

This paper investigates the effects of inlet turbulence conditions and near-wall treatment methods on the heat transfer prediction of gas turbine vanes within the range of engine relevant turbulence conditions. The two near-wall treatment methods, the wall-function and low-Reynolds number method, were combined with the SST and ωRSM turbulence model. Additionally, the RNG k-ε, SSG RSM, and SST+γ-Re_θ transition model were adopted for the purpose of comparison. All computations were conducted using a commercial CFD code, CFX, considering a three-dimensional, steady, compressible flow. The conjugate heat transfer method was applied to all simulation cases with internally cooled NASA turbine vanes. The CFD results at mid-span were compared with the measured data under different inlet turbulence conditions. In the SST solutions, on the pressure side, both the wall-function and low-Reynolds number method exhibited a reasonable agreement with the measured data. On the suction side, however, both wall-function and low-Reynolds number method failed to predict the variations of heat transfer coefficient and temperature caused by boundary layer flow transition. In the ωRSM results, the wall-function showed reasonable predictions for both the heat transfer coefficient and temperature variations including flow transition onset on suction side, but, low-Reynolds methods did not properly capture the variation of the heat transfer coefficient. The SST+γ-Re_θ transition model showed variation of the heat transfer coefficient on the transition regions, but did not capture the proper transition onset location, and was found to be much more sensitive to the inlet turbulence length scale. Overall, the Reynolds stress model and wall function configuration showed the reasonable predictions in presented cases.

Key words: Near-wall Treatment Methods, Gas Turbine Vane, Computational Fluids Dynamics

Nomenclature

C	Vane axial chord length, [m]
C_μ	Turbulence model (k-ε) constant, [0.09]
H	Heat transfer coefficient, [W/m²K]
k	Turbulence kinetic energy, [m²/s²]
L_T	Turbulence length scale, [m]
M	Mach number
$\dot{m}$	Mass flow rate, [kg/s]
P	Pressure, [kPa]
Pr	Fluid Prandtl number, $\mu c_p/\lambda$
q	Heat flux, [W/m²]
Re	Reynolds number
T	Temperature, [K]
Tu	Turbulence intensity, [%]

* Graduate student, d.eng@hotmail.com
** Professor, Corresponding author: jscho@hanyang.ac.kr
*** Researcher, Seawook.lee@ryerson.ca
**** Researcher, electra@kari.re.kr

Received: August 10, 2015 Revised: March 7, 2016 Accepted: March 8, 2016

http://ijass.org pISSN: 2093-274x eISSN: 2093-2480

U	Velocity magnitude, [m/s]
x	X-direction (axial) distance, [m]
y	Distance from the wall, [m]
ε	Turbulence dissipation, [m^2/s^3]
ρ	Density, [kg/m^3]
λ	Thermal conductivity, [W/mK]
μ	Molecular dynamic viscosity, [kg/ms]
μ_t	Turbulent viscosity, [kg/ms]
v	Kinematic viscosity, [m^2/s]

Subscripts

D	Diameter of coolant channel
f	Fluids side
Ref.	Reference value for normalization
S	Static value
T	Total value
w	Wall side
1	Inlet
2	Outlet

1. Introduction

Increasing the turbine inlet temperature (TIT) has become a key objective in improving the efficiency and performance of gas turbine engines. In modern gas turbines, the TIT often exceeds the allowable temperature of metal components [1]. To secure the integrity and to maintain an adequate lifespan for the components, sophisticated cooling design are necessary. During the design phase of cooled vanes, the predictions of heat transfer represent one of the most important tasks [2]. Nowadays, it is typically accomplished with computational fluid dynamics (CFD) tools based on Reynolds averaged Navier-Stokes (RANS) equation systems. The RANS CFD tools have been providing a reasonable degree of accuracy for prediction of the thermal and blade loading in turbine blade rows. With a conjugate heat transfer (CHT) methodology, the RANS CFD tools are routinely used in aero and thermal design processes [3, 4]. These trends have been accelerating with recent advance in computational performance.

However, newly designed components are frequently simulated with lack of accurate inlet turbulence conditions such as turbulence intensity and length scale. Moreover the designer still faces numerous simulation cases within a short turnaround time [5]. To reduce the computational time, simulations are often conducted with a relatively coarse grid and wall-function approach, and inlet boundary conditions are specified based on earlier experimental datasets or designer's experience. Consequently, the uncertainties in the predictions of vane heat transfer remain substantial.

Although the near-wall treatment methods and inlet boundary conditions in a turbulence model have a huge impact on boundary layer flow and the heat transfer prediction for gas turbine vanes, a little attention has been paid on how near-wall treatment methods influence heat transfer predictions by the range of engine relevant turbulence levels and scales.

For the near-wall treatment methods, normally, two approaches haven been extensively used, the wall-function (WF) and low Reynolds number (LRN) method. The WF (typically y+ = 30-100) does not require fine grids in near-wall. It uses the empirical formula based on "the law of the wall" rather than direct computation of the boundary layer in the near-wall region [6]. The WF is often considered as an inferior method to the LRN method (typically y+~ 1, also known as the wall-integration approach). The LRN may provide higher accuracy by resolving the details of the boundary layer profile in the viscous sublayer [6]. However, some practices indicate that the LRN has not shown better accuracy than the WF, especially with low Reynolds number k-ε turbulence model [7]. Additionally, the LRN requires more computational runtime owing to its very fine mesh in the near-wall region.

In view of the turbulence levels and scales, inlet turbulence conditions directly affect the boundary layer flow, especially, the laminar to turbulent transition that augments the heat transfer on the vane surface [8]. To understand its effects on turbine vane, several research groups [8-10] have performed heat transfer experiments and numerical analyses. Nasir et al. [10] investigated the effects of free stream turbulence and length scales, both experimentally and numerically, in transonic cascade facilities. They made several comparisons between the data and numerical predictions using the FLUENT v^2-f model. The v^2-f model predicted reasonably the heat transfer coefficient (HTC) at low free stream turbulence levels. At high free stream turbulence levels, the HTC was found to be significantly over predicted on the vane surface. However, the v^2-f model does not support the WF, because the v^2-f model was originally developed to capture the near-wall flow behaviors. Although the v^2-f model provides substantially improved predictions for heat transfer [11], it is not adequate for reasonable predictions in case of relatively coarse grids. The near-wall grid requirement of the v^2-f model make computation and grid generation cost prohibitively expensive or impossible in complex 3D geometry such as film cooled components.

Recently, Luo et al. [12] compared the near-wall treatment

effects for turbine vanes and end-walls. They showed that the WF provided a significantly reduced sensitivity to the inlet turbulence length scale for the HTC results when k-ε turbulence model is specified. They also showed that WF solution with k-ω based shear stress transport (SST) turbulence model was found to be comparable to the LRN solutions. However, their study was conducted with an adiabatic wall condition. This setup is insufficient for understanding the effect of inlet turbulence condition on heat transfer prediction in the CHT simulation. Ledezma et al. [5], who performed the CHT simulation using the NASA C3X vane, showed that the SST model has better agreement with the experimental data than the ωRSM. However, they only focused on the LRN solutions without WF.

This paper focusses on the effect of the near-wall treatment methods and inlet turbulence conditions on the heat transfer prediction of the gas turbine vane in the range of relevant engine turbulence conditions. Two extensively used near-wall treatment methods were evaluated with four turbulence model. Since boundary layer transition strongly affects the heat transfer, the γ-Re_θ transition model also was compared. The CHT method was applied to all simulation cases, and results were compared and discussed with the experimental data of the NASA C3X and MarkII vane.

2. Numerical Methods

2.1 Models

The NASA C3X and MarkII transonic turbine vane experimental datasets provided by Hylton et al. [13] were selected for validation purposes. The cross section of the C3X and MarkII at mid-span are shown in Fig. 1 along with the configuration of the coolant channels. The experiment had been performed using a linear cascade with three vanes, and each of the vanes was cooled by air through ten radial cooling channels. The coolant channels of the outer two vanes were connected to a common plenum. Whereas each coolant channel of the middle vane was supplied from a separated coolant source for measurements. The geometric parameters of C3X and MarkII vane are listed in Table 1.

The 3D computational domains were composed of three parts, the hot gas passage, solid vane, and coolant channels. An isoview of the computational domains of C3X vane is presented in Fig. 2. The domains of MarkII are not shown here, because they have the same configuration as the C3X domains. The hot gas inlet was located at 180mm (about 2 times the axial chord length) upstream of the leading edge (LE). This position was sufficient to attain a fully developed flow, and was same as the position of the pressure sensor taps in the test section. The hot gas outlet was located at 240 mm downstream of the trailing edge (TE). The coolant

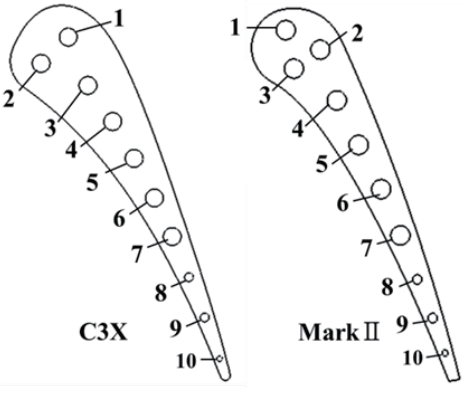

Fig. 1. C3X (left) and MarkII (right) vane profile

Table 1. Geometry parameters of vanes

Parameters	MarkII	C3X
Stagger angle (deg.)	63.69	59.89
Air exit angle (deg.)	70.96	72.38
Throat (mm)	39.83	32.92
Vane spacing (mm)	129.74	117.73
Vane height (mm)	76.2	76.2
True chord (mm)	136.22	144.93
Axial chord (mm)	68.55	78.16

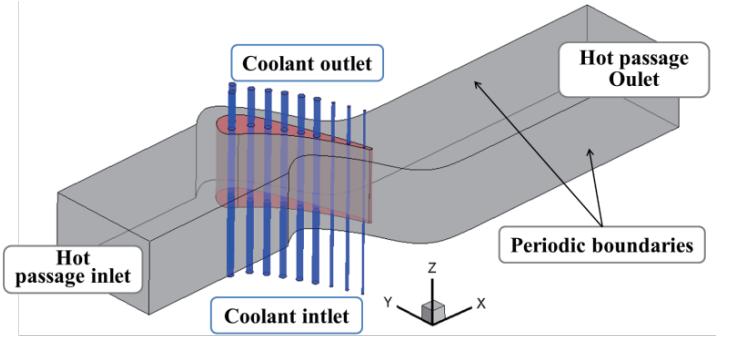

Fig. 2. Computational domains of C3X vane

inlet was extended by 76.2 mm (about 13 times the channel diameter) from the hub, and the outlet was located at 36 mm from the shroud.

2.2 RANS solvers and boundary conditions

ANSYS CFX academic V14.5, the commercial CFD tool, was used to solve the system of the 3D RANS equations. CFX is a fully implicit pressure based coupled solver with a co-located (non-staggered) finite volume method. For the pressure-velocity coupling, it uses the similar method to that proposed by Rhie and Chow [14]. In order to avoid numerical instabilities in the shock wave regions, the limiter proposed by Barth and Jesperson [15] is used. For the convergence acceleration, an anisotropic algebraic multigrid method proposed by Raw was used [16]. The detailed information on solver algorithms can be found in the CFX theory book. [17].

In this study, all governing equations were discretized using high-resolution scheme, which provides a second order accuracy. The root mean square (RMS) residual and domain imbalances were used as convergence criteria. To check the steady-state solutions, Mach number was monitored at each domain outlet. The converged solutions were obtained when RMS residual was less than 1.0E-5 for all independent variables. However, some simulation cases that use Reynolds stress turbulence model were less than 5.0E-5. Nevertheless global imbalances in each domain for all simulation cases made less than 0.1% which indicates that conservation had been achieved.

The inlet boundary conditions of the hot gas passage were specified as total pressure, total temperature, turbulence intensity, and length scale. The mass flow rate and the total temperatures were prescribed at inlet of coolant channel. The static pressure was imposed at the outlets of hot gas passage and each coolant channel. The periodic boundary condition with a 1:1 nodal connectivity was set along the periodic plane in order to reduce the problem size. The general grid interface (GGI) was specified to all fluid-solid interfaces owing to its existing of non-conformal nodes.

Two subsonic operating conditions were selected for the C3X vane. The conditions are the same as the experiment code Run148 and Run158 provided by Hylton et al. [13]. These two conditions are essentially identical except for inlet turbulence intensity of the hot passage. Contrary to this case, the MarkII vane was only simulated using a Run46 condition. For the evaluation of geometrical effects, the Run46 condition was selected owing to the fact that it is fairly consistent with the Run148 conditions of the C3X vane. The detailed operating and boundary conditions are listed in Table 2 and Table 3.

Table 2. Hot passage flow conditions

Case No. / (Vane & Exp. Code)	P_{T1} (kPa)	T_{T1} (K)	Tu_1 (%)	L_{T1} (mm)	M_1	Re_1	P_{S2} (kPa)	M_2	Re_2
1 / (C3X & Run158)	243.45	808	8.3	0.4, 16, auto compute	0.17	0.38E+06	180	0.91	1.47E+06
2 / (C3X & Run148)	244.76	802	6.5	0.4, 16, auto compute	0.17	0.39E+06	180	0.91	1.49E+06
3 / (MarkII & Run46)	276.48	803	6.5	0.4, 16, auto compute	0.18	0.45E+06	163.5	0.90	1.56E+06

Table 3. Coolant flow conditions

Coolant Channel No.	Case 1 (C3X & Run158)			Case 2 (C3X & Run148)			Case 3 (MarkII & Run46)		
	$\dot{m}$ (kg/s)	Re_D	T_{T1} (K)	$\dot{m}$ (kg/s)	Re_D	T_{T1} (K)	$\dot{m}$ (kg/s)	Re_D	T_{T1} (K)
1	1.67E-02	15.99E+04	348.5	1.62E-02	15.49E+04	351.0	1.55E-02	15.27E+04	335.0
2	1.74E-02	16.62E+04	350.5	1.69E-02	16.16E+04	352.0	1.53E-02	15.40E+04	327.0
3	1.48E-02	14.44E+04	341.0	1.62E-02	15.97E+04	338.0	1.51E-02	14.95E+04	333.0
4	1.65E-02	16.02E+04	342.5	1.64E-02	15.87E+04	343.5	1.60E-02	15.58E+04	342.0
5	1.75E-02	17.34E+04	333.0	1.72E-02	17.07E+04	332.5	1.52E-02	15.60E+04	316.0
6	1.65E-02	15.38E+04	362.5	1.76E-02	16.15E+04	371.0	1.50E-02	15.55E+04	311.5
7	1.61E-02	15.65E+04	340.5	1.67E-02	16.23E+04	342.0	1.54E-02	15.47E+04	324.5
8	0.550E-02	10.09E+04	363.0	0.570E-02	10.43E+04	365.0	0.508E-02	9.54E+04	349.0
9	0.349E-02	6.10E+04	384.5	0.371E-02	6.39E+04	394.5	0.333E-02	5.87E+04	332.0
10	0.171E-02	4.41E+04	411.5	0.185E-02	4.68E+04	424.0	0.227E-02	5.84E+04	387.0

Although Hylton et al. [13] reported the detailed operating conditions of experiments. They did not describe the outlet pressure of hot passage and coolant channel, and the inlet total temperature of coolant channel. Therefore, these unknown conditions were specified to match the corresponding Reynolds number and mid-span total temperature within the experimental uncertainty.

The inlet turbulence length scale, LT (also, unknown from [13]), was set to a value of earlier researches [7, 18], and to a value based on the equation (2). When the specific turbulence length scale was defined, the inlet turbulence dissipation was calculated by

$$\varepsilon_1 = \frac{k^{3/2}}{L_T} \tag{1}$$

On the other hand, only intensity was specified, the value can be defined as

$$\varepsilon_1 = \rho C_\mu \frac{k^2}{\mu_T} \tag{2}$$

where : μ_t=1000$\mu \cdot Tu$

The working fluid was specified to air based on the ideal gas law. The molecular viscosity and thermal conductivity were specified as functions of temperature using Sutherland's formula and based on kinetic theory [19], respectively. The specific heat capacity at constant pressure was specified as a function of temperature, which is 4th order polynomial, since it varied significantly over a range of different temperatures. The vanes were fabricated with ASTM 310 stainless steel, which has a relatively low thermal conductivity. The material has a constant density of ρ=7900 kg/m^3, and a specific heat of C_p=586.15 J/kgK. The thermal conductivity was specified as λ=0.02017T+6.811 W/mK [18].

2.3 Turbulence models and near-wall treatment methods

The combination of four turbulence models and two near-wall treatment methods were selected in this study. In CFX, only the turbulence models based on the ω-equation were allowed for the LRN method owing to the deficiency and numerical instability in low Reynolds number turbulent flows, in case when the ε-based turbulent model was specified [17]. Nevertheless, the ε-based high Reynolds number turbulence models were adopted for the purpose of comparison. The detailed combinations are described in Table 4. The RNG k-ε, SST, ωRSM, and Reynolds stress model by Speziale, Sarka, and Gatski (SSG RSM) [20]. The LRN method was only employed for the SST and ωRSM turbulence model, whereas a scalable WF was used in all turbulence models. Additionally, the γ-Re_θ transition model, proposed by Menter et al. [21], was used with the SST model. Because it is known to be able to capture bypass transition [5, 21], that is one of the key feature for turbine vane heat transfer predictions.

The scalable WF is essentially identical with the standard WF based on the law of the wall. However, the scalable WF limited the minimum y+ value less than 11.06, which is the intersection value between the logarithm law and the linear near-wall profile [17]. It overcomes the numerical instability of the standard WF, when it computes the very fine grid at the near-wall. The major advantage of the WF is that it can resolve the high gradient shear stress layer in the near-wall regions using a relatively coarse grid [22]. On the other hand, the LRN method resolves the details of the boundary layer profile by using very fine grids in near-wall region. It can present the viscous effects near the wall, and may provide variation of flow information with a higher accuracy. However, it requires relatively high computational resources and runtime.

The thermal boundary layer is computed using the thermal law of the wall function proposed by B.A. Kader [23]. The non-dimensional near-wall temperature, T^+, for the LRN method is defined as

$$T^+ = \Pr y^* e^{-\Gamma} + [2.12\ln(y^*) + \beta] e^{(-1/\Gamma)} \tag{3}$$

Where ;

$$\beta = (3.85\,\Pr^{1/3} - 1.3)^2 + 2.12\ln(\Pr) \tag{4}$$

$$\Gamma = \frac{0.01(\Pr y^*)^4}{1 + 5\,\Pr^3 y^*} \tag{5}$$

$$y^* = \frac{u^* \Delta y}{\nu} \tag{6}$$

Table 4. Turbulence models and near-wall treatment methods

Turbulence model	Wall-function method	Low Reynolds number method	Transition model
RNG k-ε	Scalable wall-function	-	-
SST		Automatic near-wall treatment	γ-Re_θ model
ωRSM		Automatic near-wall treatment	-
SSG RSM		-	-

$$u^* = C_\mu^{1/4} k^{1/2} \tag{7}$$

y^* is non-dimensional near-wall distance, and u^* is alternative velocity scale that is used in solver instead of conventional formula of friction velocity to avoid singularity problem. For the scalable WF method, is defined as

$$T^+ = 2.12 \ln(y^*) + \beta \tag{8}$$

Then, the heat flux at the wall and fluid interface is calculated as

$$q_w = \frac{\rho c_p u^*}{T^+}(T_w - T_f) \tag{9}$$

When the very fine grid in the near-wall is used in CFX, the near wall treatment methods are automatically switched from WF to low-Reynolds formulations, named as the automatic wall treatment [17, 24]. However, it is not possible for the user to select the LRN method. Instead solver activates and deactivates the near-wall treatment methods depending on the local y+ value. Therefore, the near-wall treatment methods are dependent on the computational input mesh.

The computational meshes for C3X vane are shown in Fig. 3. The maximum y+ value of the computational mesh for WF and LRN was calculated as 50 and 1, respectively. The mesh for the MarkII vane is not presented here, owing to same block topology and mesh configurations of the C3X vane. Since the C3X and MarkII Vanes had a constant cross section, a 2D mesh was first created using the blocking method with the ICEM CFD meshing software. Then, 3D mesh was generated by stacking the 2D meshes, after the mesh was stretched to improve orthogonality. In the C3X vane case, the number of elements for WF and LRN were 2.6 million and 7.2 million cells, respectively. For the MarkII vane, the element counts of WF and LRN method were 2.4 million and 5.9 million cells, respectively. The grid independent test was performed with various streamwise node densities at given y+ values. The final node count distributions are listed in Table 5.

3. Results and Discussions

The results of the CHT simulation are presented and analyzed in this section, under the three flow conditions, as listed in Tables 2 and 3. The pressure loadings, external HTC, and temperature are compared with the measured data from Hylton et al. [13]. In this study, "WF" is used as a suffix for the turbulence model with wall-function method (e.g., SST_WF), while "LRN" is used for low-Reynolds number method (e.g., SST_LRN). For the RNG k-ε and SSG_RSM model, default name is used as listed in Table 4.

3.1 Pressure loadings

The predicted and measured pressure distributions on the entire vane surface at the mid-span are shown in Fig. 4. For the C3X vane, only results of Case1 are plotted, because Case1 (Exp. Run158) and Case2 (Exp. Run148) results were essentially identical.

The pressure predictions from the all the presented turbulence models are in excellent agreement with the measurements for both the C3X and MarkII vanes. However, on the suction side of the C3X vane, the discrepancy is observed between the measured data and predictions in $0.7 \le x/C \le 1.0$. In this region, the gas flow acceleration seems to be higher compared to experiments. Thus, the pressure falls rapidly and the simulation has predicted the presence of the strong shock that is not observed in the measurements. On the other hand, the pressure prediction for MarkII on the suction side exhibit good agreement with the measurements. A strong adverse pressure gradient due to a weak shock is also

Table 5. Node count of vanes

Parameters	MarkII		C3X	
	WF	LRN	WF	LRN
Airfoil	253	283	307	351
Spanwise	51	79	55	99
Blade-to-blade	73	131	95	179

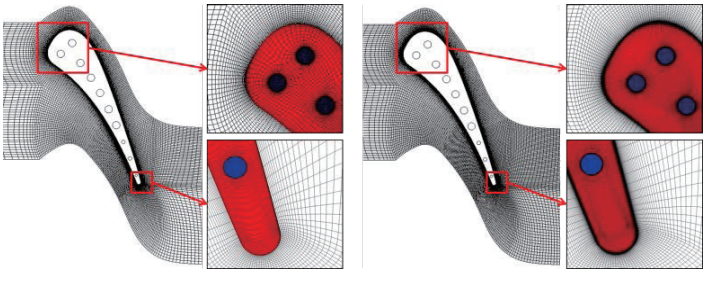

Fig. 3. Computational mesh for the WF (left) and LRN (right) of C3X vane

represented very well with the presented turbulence model. It should be noted that the WF and the LRN yield almost identical results for the prediction of pressure loadings, including transition model owing to the no flow separation on the vane.

3.2 Effects of near-wall treatment methods

The normalized HTC and temperature distributions on the C3X vane surface at the mid-span are shown in Fig. 5 and 6, respectively. In the SST solution, both WF and LRN method exhibit a reasonable agreement with measurements on the pressure side and on the portion of the suction side x/C≥0.6. In the presented SST case, the near-wall treatment methods do not seem to significantly affect the HTC and temperature. The RNG k-ε predictions also agree with experimental data exception of the portion of the curve 0.1≤x/C≤0.6. In regards to the temperature predictions, the

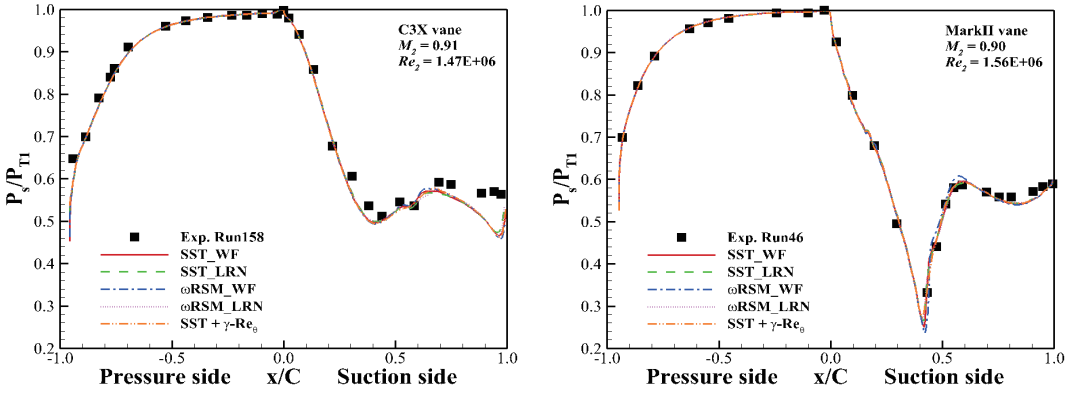

Fig. 4. Pressure distribution of C3X vane (left) and MarkII vane (right) at midspan

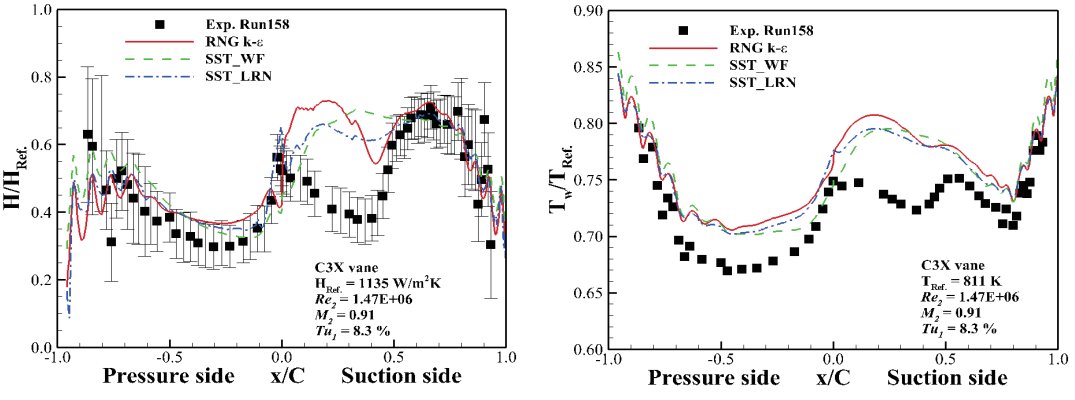

Fig. 5. HTC (left) and temperature (right) distributions from the RNG k-ε and SST model at the midspan

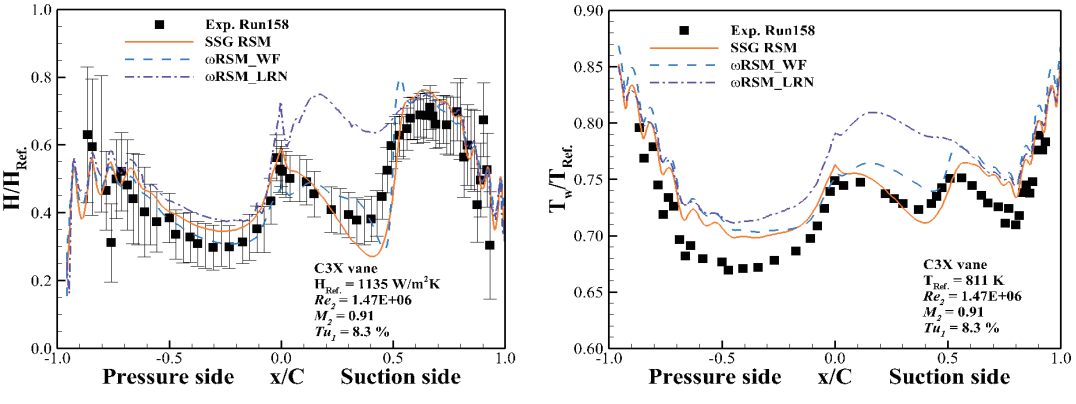

Fig. 6. HTC (left) and temperature (right) distributions from the SSG RSM and ωRSM at the midspan

DOI: http://dx.doi.org/10.5139/IJASS.2016.17.1.8

difference between the SST_LRN and SST_WF are less than 2%. For the HTC predictions, the SST_LRN and SST_WF yield similar results, although the SST_WF slightly underestimates the HTC around the LE -0.1≤x/C≤0.1 with an error of 20%, compared to experimental measurements. Even considering the large uncertainties of HTC measurements, however, the results from the SST in Fig. 5 show excessive overpredictions for the temperature and the HTC around two data points 0.1≤x/C≤0.6. These discrepancies are mainly due to the boundary layer transition as observed and discussed by the other researches [5, 18].

In consideration of the Reynolds number in the C3X vane, it is fact that the flow is apparently laminar at the LE and towards as transition to turbulent at the downstream locations in the near-wall. Since the WF computes the boundary layer considering fully turbulent flow, the WF with the SST model is not proper to compute the laminar and transition flow regimes. The LRN with the SST model was also originally developed for fully turbulent flows [24], consequently, it yields as same prediction as the WF.

On the other hand, the near-wall treatment methods with the RSM model exhibit the significant differences in both HTC and temperature in Fig. 6. The ωRSM_WF predictions are in good agreement with the measured temperature in the quasi-laminar and transition flow region on the entire vane surface, within an error of 3%. The HTC results are also in reasonable agreement with the measured data within the range of uncertainties. The SSG RSM model, that uses only wall-function, also yields a good agreement with variation of the HTC and temperature along the axial chord. However, the ωRSM_LRN did not capture the slope of the variations in both the HTC and temperature. These results would be caused by over productions of turbulence kinetic energy in the near-wall regions.

The contours of the turbulence kinetic energy at the mid-span for Case1 are shown in Fig. 7. The ωRSM_LRN prediction in Fig. 7b shows a higher turbulence kinetic energy than that of the ωRSM_WF prediction in Fig. 7a at the data point x/C = 0.314 on the vane surface. Due to the influence of low-Reynolds formulation of the ω-equation, the turbulence kinetic energy based on ωRSM_LRN yields similar results compared to the SST_LRN results as shown in Fig. 7c at the boundary layer. This turbulence kinetic energy affects the thermal boundary layer profile significantly.

Figure 8 and 9 show the alternative velocity scale, u^*, by eq. (7), and temperature profile at the position x/C = 0.314, respectively. The alternative velocity scale u^* is related to kinetic energy and uses to calculate the non-dimensional temperature profile, T^+, and wall heat flux. Consequently, to get accurate temperature profile, accurate u^* calculation is necessary. In the Fig. 8, the value of u^* indicates higher value in LRN solution compared to WF and γ-Re_θ solutions. Consideration of the position x/C = 0.314, flows seem to be laminar flow regime. Hence, these strong u^* values are not adequate to compute the thermal boundary layer profile, and they elicit the higher temperature predictions as shown in Fig. 9. The SSG RSM and ωRSM_WF yield reasonable kinetic energy values, consequently, temperature predictions of these models are in good agreement with experiments near the x/C = 0.314.

Theoretically the Reynolds stress models have shown more reasonable prediction performance for complex flow compared to eddy-viscosity models. These models solve the transport equations directly for individual components of the Reynolds stress tensor without consideration of the Boussinesq eddy-viscosity assumption. However, reasonable predictions by the Reynolds stress model seem to be valid

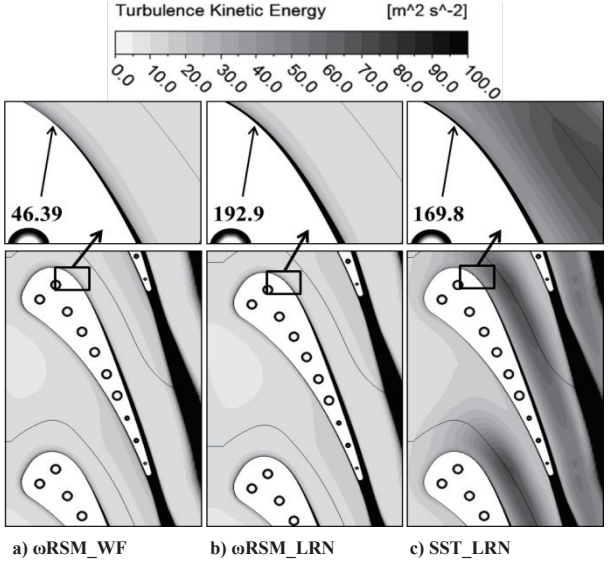

Fig. 7. Turbulent kinetic energy contours at the midspan

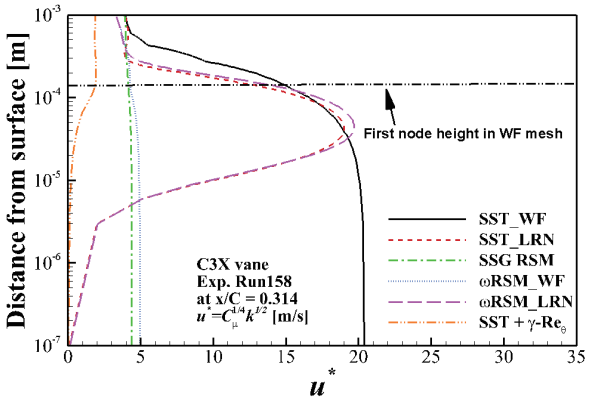

Fig. 8. Alternative velocity profile at x/C=0.314 on the vane suction side

only with WF, and considering the ωRSM_LRN solutions, not the results by a physical modeling of transition process, seems to be based on the reasonable production of turbulent kinetic energy.

Figure 10 shows the predictions from the γ-Re_θ model with the measured data. The HTC and temperature predictions are poorly predicted in both the pressure and suctions side, respectively, compared to measurements. Due to the favorable pressure gradient on the vane pressure side, the γ-Re_θ model does not trigger the onset of the transition process, and the entire pressure side seems to compute as laminar flow. This transition model does not represent the physics of the transition process, but it modeled a transition process based on experimental correlation. Consequently, the γ-Re_θ model does not properly predict the transition onset location on the suction side, and underpredict the HTC in the presented case.

Contrary to this result, one equation version of the γ-Re_θ model, called as γ-model, yields the more favorable agreement with the measured HTC on the pressure side than the γ-Re_θ model, by assuming the onset Re_θ as 90 throughout the entire hot passage domain. Nevertheless, it still yields underpredictions of the HTC with error of 20%. For the γ-model, the good agreement with the measured temperature is acquired at the onset Re_θ = 150, although the HTC is not correctly computed on the pressure side. However, the γ-model can provides the improved temperature predictions compared to the fully turbulent SST model. It is difficult to determine the proper onset Re_θ value for simultaneously modeling the transition on both the pressure and suction side, especially in initial design phase.

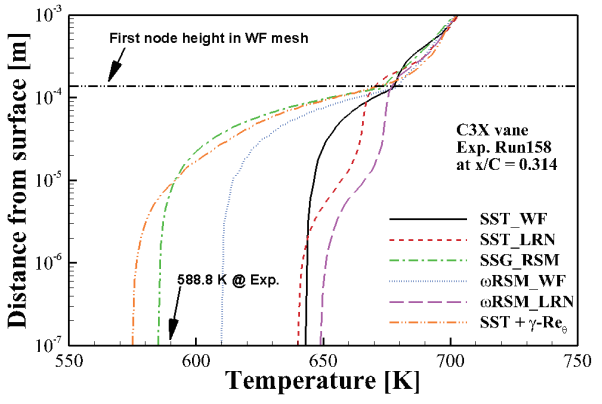

Fig. 9. Near-wall temperature profile at x/C=0.314 on the vane suction side

3.3 Effects of inlet turbulence intensity and length scale

The effects of the inlet turbulence intensity level on the heat transfer of the C3X vane are presented in Fig. 11. The specified turbulence intensity levels were 8.3% and 6.5% as listed in Table 2. In the SST solutions in Fig. 11a, on the pressure side, both the WF and LRN did not show the detailed difference of the HTC by the inlet turbulence intensity level with compared to the measured data. On the other hand, on the suction side, both the WF and LRN can yield a detailed discrepancy of the HTC by inlet turbulence intensity level. In the ωRSM solutions in Fig. 11b, only the LRN solutions show the detailed difference of the HTC by inlet turbulence intensity, while they still indicate poor HTC predictions on the transition flow region. The γ-Re_θ transition model, including the γ-model, does not yield a difference of HTC by inlet turbulence intensity level on both the pressure and suction side.

However, in the fully turbulent flow region on the suction side in x/C≥0.6, the HTC discrepancy is not much clear in the both the measurements and the present HTC predictions in the Fig. 11, and both the WF and LRN yield the very similar HTC predictions. The inlet turbulence intensity level only seems to affect the position of the transition onset

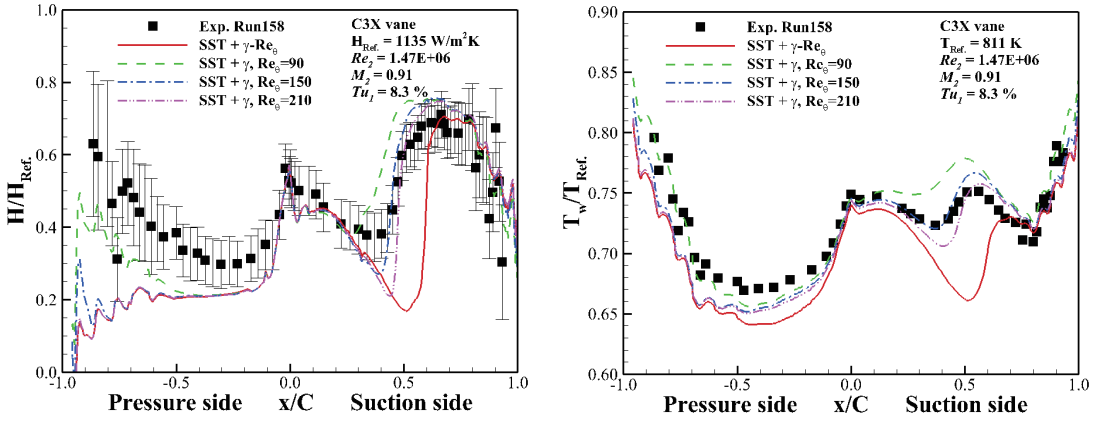

Fig. 10. HTC (left) and temperature distributions from the SST+γ-Re_θ model

location and the HTC augmentation on quasi-laminar and transitional flow regions.

The effects of the inlet turbulence length scale on the HTC distribution for the C3X vane are plotted in Fig. 12. Since the inlet turbulence length scale is not described in Ref. [12], an arbitrary value was specified as listed in Table 2. In the SST solutions in Fig. 12a, on the pressure side, the SST_LRN does not model the detailed difference of HTC augmentation by inlet turbulence length scale. On the other hand, the SST_WF capture the detailed discrepancy of HTC by inlet turbulence length scale on the entire midspan. In the ωRSM solutions in Fig. 12b, both the LRN and WF capture the difference of HTC by the inlet turbulence length scale. However, the HTC augmentation by the ωRSM_LRN on the LE is much severe than the SST_LRN solution, especially with case of L_T=16mm. On the entire vane surface, the bigger turbulence scale resulted in elevation of the HTC. However, the predictions by the γ-Re_θ model in Fig. 12c is in very poor agreement with measured data at L_T = 0.4mm, while the SST and ωRSM solutions indicate reasonable predictions.

3.4 Results from other cases

The HTC and temperature predictions from Case2 (C3X) and Case3 (MarkII) are plotted in Fig. 13 and 14, respectively. These two cases have essentially identical flow conditions for the hot passage as listed in Table 2. Based on the comparison of the near-wall treatment methods with turbulence model for Case1 listed above, it was concluded that the WF can provide sufficient and reasonable predictions. Therefore in this section, the predictions of the WF and the γ-Re_θ model (for the purpose of comparison) are presented. For Case2 in Fig. 13, the best agreement with the measurements is obtained using by the SSG RSM model. The ωRSM_WF predictions also showed good agreement with both the measured HTC and temperature within an error of 4%.

For the MarkII vane of Case3 in Fig. 14, the HTC predictions by the SSG RSM and ωRSM_WF are in good agreement with the experimental data. Nevertheless, these two turbulence models strongly overestimated the HTC on the suction side around the point x/C=0.6. The HTC predictions from the SST_WF are reasonably matched with experiments data except for laminar and transition region 0≤x/C≤0.45. For the γ-Re_θ model, the HTC values are underpredicted on the pressure side, and overpredicted at x/C=0.6.

4. Conclusions

The 3D RANS analyses were performed to evaluate the effect of near-wall treatment methods and inlet turbulence conditions. The conjugate heat transfer methodology was

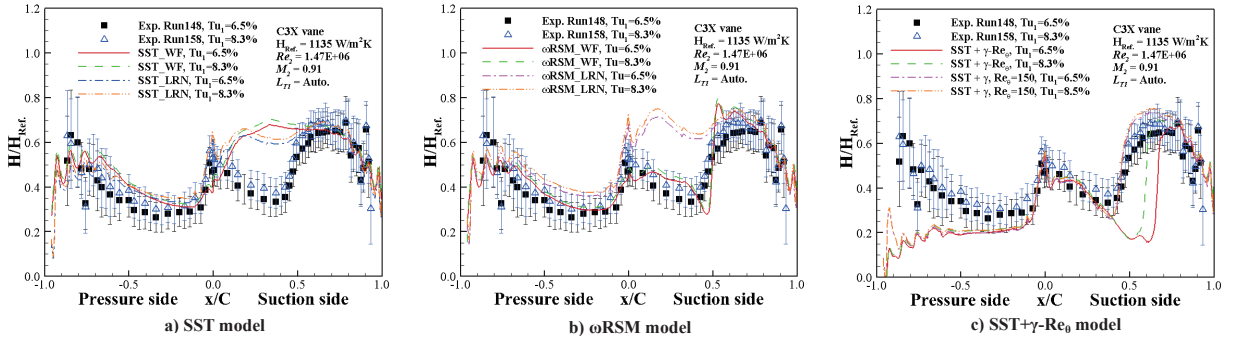

Fig. 11. Effects of the inlet turbulence intensity level

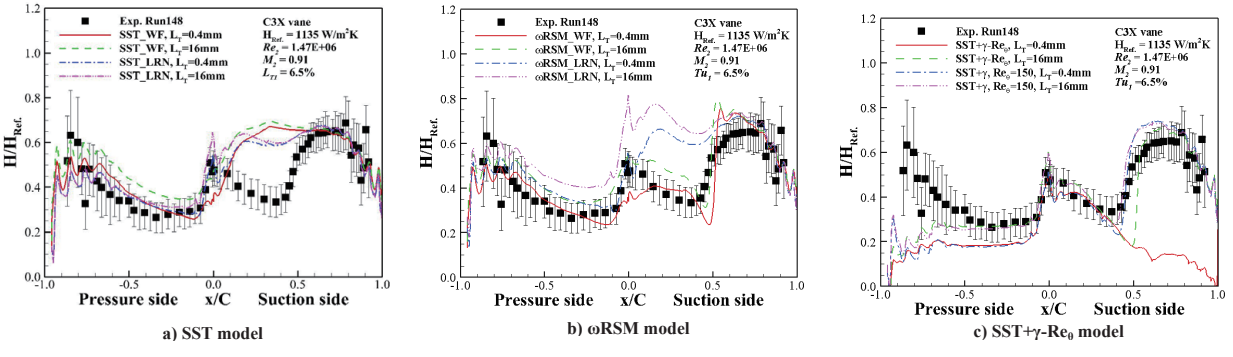

Fig. 12. Effects of the inlet turbulence length scale

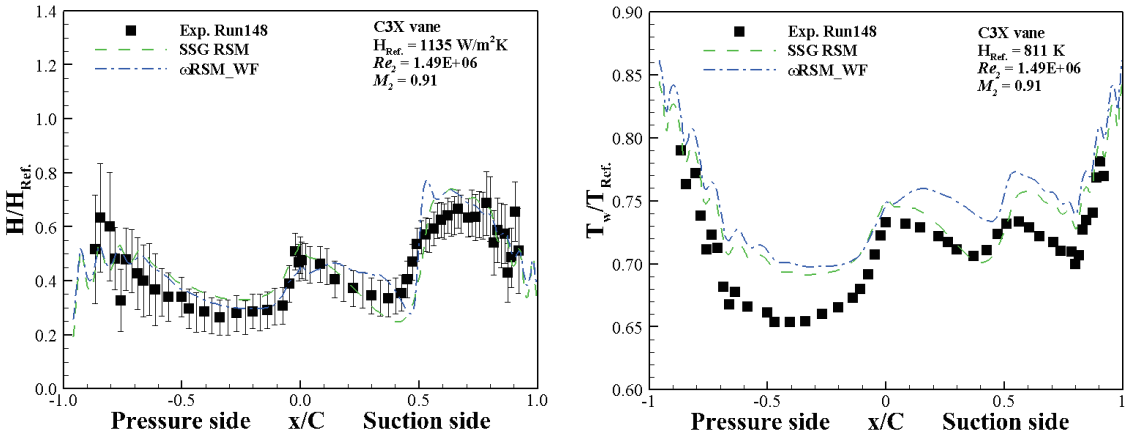

Fig. 13. HTC (left) and temperature (right) distributions from the Case 2 (C3X vane) at the midspan

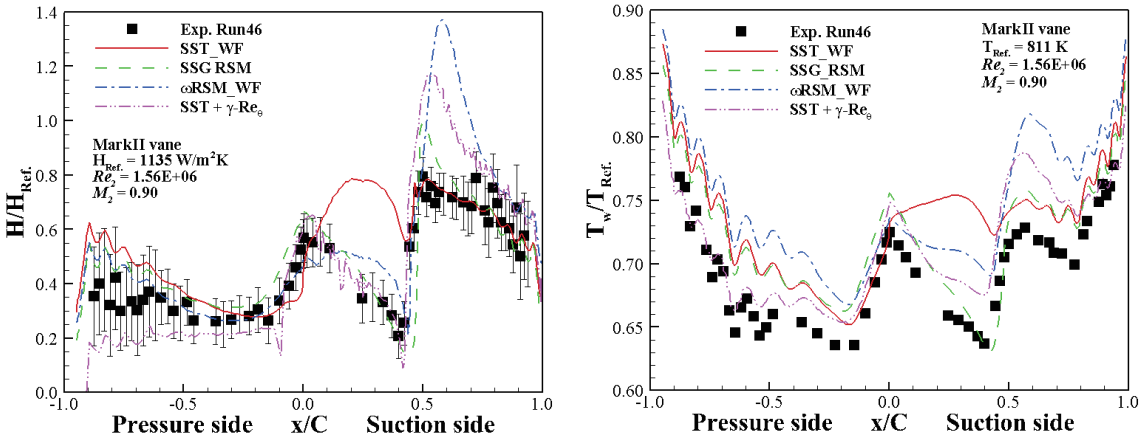

Fig. 14. HTC (left) and temperature (right) distributions from the Case 3 (MarkII vane) at the midspan

applied to the NASA C3X and MarkII vanes with realistic engine-like flow conditions.

The low Reynolds number methods was only employed to the SST and ωRSM turbulence model whereas a scalable wall-function was used to the all presented turbulence models (RNG k-ε, SSG RSM, SST and ωRSM). The predicted results were clearly affected by the combination of the near-wall treatment method and turbulence model.

For the SST solutions, the WF was found to provide very similar HTC and temperature prediction compare to the LRN. In the laminar-turbulent transition region, both the WF and LRN overpredicted HTC and temperature, however, in other regions, it provided reasonable predictions including the detailed difference of the HTC by the inlet turbulence intensity level.

For the RSM solutions, the WF showed the best accuracy for both the HTC and temperature prediction, however, did not capture the detailed difference of the HTC by inlet turbulence intensity level. In considering the ωRSM_LRN solutions, the reasonable prediction by the RSM_WF is not the results by a physical modeling of transition process, only seems to be based on the reasonable production of turbulent kinetic energy.

The γ-Re_θ model including theγ-model showed a better accuracy than the fully turbulent SST model. It presented the temperature and HTC variations along the axial chord due to the boundary layer transition, however, underpredicted the HTC and temperature with an error of 30% and 10%, respectively. The γ-Re_θ model did not capture the detailed difference of the HTC by the inlet turbulence intensity and length scale.

The selection of the appropriate turbulence model and near-wall treatment for the gas turbine heat transfer problem is always a burdensome task for engineers within the short turnaround time. It is believed that present results can give some insight for selecting a turbulence models and near-wall treatments for calculating the heat transfer problem on the gas turbine vane. Further studies are needed for film cooling

and at various turbulence intensity levels considering the combustion systems.

Acknowledgement

This work was supported by Korea Aerospace Technology Research Association (KATRA) and Ministry of Trade, Industry, and Energy (MOTIE).

References

[1] Ralf, S. and Sigmar, W., "Gas Turbine Heat Transfer: Past and Future Challenges", *Journal of Propulsion and Power*, Vol. 16, No. 4, 2000, pp. 583-589.

[2] Han, J. C., Dutta, S. and Ekkad, S. V., *Gas Turbine Heat Transfer and Cooling Technology*, 1st ed., Taylor and Francis, London, 2000.

[3] Facchini, B., Magi, A. and Greco, A. S. D., "Conjugate Heat Transfer Simulation of a Radially Cooled Gas Turbine Vane", *ASME Paper*, No. GT2004-54213, 2004.

[4] Tucker, P. G., "Trends in Turbomachinery Turbulence Treatments", *Progress in Aerospace Sciences*, Vol. 63, 2013, pp. 1-32.

[5] Ledezma, G. A., Laskowski, G. M. and Tolpadi, A. K., "Turbulence Model Assessment for Conjugate Heat Transfer in a High Pressure Turbine Vane Model", *ASME Paper*, No. GT2008-50498, 2008.

[6] Wilcox, D. C., *Turbulence Modeling for CFD*, 2nd ed., DCW industries, La Canada, CA, 1998.

[7] Luo, J. and Razinsky, E. H., "Conjugate Heat Transfer Analysis of a Cooled Turbine Vane Using the V2F Turbulence Model", *ASME Journal of Turbomachinery*, Vol. 129, No. 4, 2006, pp. 773-781.

[8] Ames, F. E., Experimental Study of Vane Heat Transfer and Aerodynamics at Elevated Levels of Turbulence, *NASA* CR-4633, 1994.

[9] Ames, F. E., "The Influence of Large-Scale High Intensity Turbulence on Vane Surface Heat Transfer", *ASME Journal of Turbomachinery.*, Vol. 119, No. 1, 1997, pp. 23-30.

[10] Nasir, S., Carullo, J. S., Ng, W., Thole, K. A., Wu, H., Zhang, L. J., and Moon, H. K., "Effects of Large Scale High Freestream Turbulence and Exit Reynolds Number on Turbine Vane Heat Transfer in a Transonic Cascade", *ASME Journal of Turbomachinery*, Vol. 131, No. 2, 2009, 021021.

[11] Medic, G. and Durbin, P. A., "Toward Improved Prediction of Heat Transfer on Turbine Blades", *ASME Journal of Turbomachinery*, Vol. 124, No. 2, 2002, pp. 187-192.

[12] Luo, J., Razinsky, E. H. and Moon. H. K., "Three-Dimensional RANS Prediction of Gas-Side Heat Transfer Coefficients on Turbine Blade and Endwall", *ASME Journal of Turbomachinery*, Vol. 135, No. 2, 2012, 021005.

[13] Hylton, L. D., Milhec, M. S., Turner, E. R., Nearly, D. A. and York, R. E., "Analytical and Experimental Evaluation of the Heat Transfer Distribution Over the Surface of Turbine Vanes", *NASA CR-168015*, 1983.

[14] Rhie, C. M. and Chow, W. L., "A numerical Study of the Turbulent Flow Past an Isolated Airfoil with the Trailing Edge Separation", *AIAA Paper*, No. 82-0998, 1982.

[15] Barth, T. J. and Jesperson, D. C., "The Design and Application of Upwind Schemes on Unstructured Meshes", *AIAA Paper*, No. 89-0366, 1989.

[16] Raw, M. J., "Robustness of Coupled Algebraic Multigrid for the Navier-Stokes Equations," AIAA 34th Aerospace and Sciences Meeting & Exhibit, *AIAA Paper*, No. 96-0297, 1996.

[17] ANSYS Inc., *ANSYS CFX-Solver Theory Guide*, Release 14.0, ANSYS Inc., Canonsburg, PA, 2011.

[18] York, W. D. and Leylek, J. H., "Three-Dimensional Conjugate Heat Transfer Simulation of an Internally-Cooled Gas Turbine Vane", *ASME Paper*, No. GT2003-38551, 2003.

[19] White, F. M., *Viscous Fluid Flow*, 3rd ed., McGraw-Hill, New York, 2006.

[20] Speziale, C. G., Sarka, S. and Gatski, T. B., "Modeling the Pressure-strain Correlation of Turbulence : An Invariant Dynamical Systems Approach", *Journal of Fluid Mechanics*, Vol. 227, 1991, pp.245-272

[21] Menter, F. R., Langtry, R.B. Likki, S. R., Suzen, Y. B., Huang, P. G. and Völker, S., "A Correlation-Based Transition Model Using Local Variables-Part I : Model Formulation", *ASME Journal of Turbomachinery*, Vol. 128, No. 3, 2006, pp. 413-422.

[22] Bredberg, J., "On the Wall Boundary Condition for Turbulence Models", Chalmers University of Technology, Department of Thermo and Fluid Dynamics, *Internal Report*, No. 00/4, Göteborg, 2003.

[23] Kader, B.A., "Temperature and concentration profiles in fully turbulent boundary layers", *International Journal of Heat and Mass Transfer*, Vol. 24, No. 9, 1981, pp. 1541-1544.

[24] Menter, F. R., Ferreira, J. C., Esch, T. and Konno, B., "The SST Turbulence Model with Improved Wall Treatment for Heat Transfer Predictions in Gas Turbines", *IGTC2003-TC-059*, 2003.